Ferroelectric and Ionic-Conductive Properties of Nonlinear-Optical Vanadate, $Ca_9Bi(VO_4)_7$

B. I. Lazoryak,*,† O. V. Baryshnikova,‡ S. Yu. Stefanovich,‡ A. P. Malakho,§ V. A. Morozov,†,|| A. A. Belik,†,# I. A. Leonidov,⊥ O. N. Leonidova,⊥ and G. Van Tendeloo||

Departments of Chemistry and Materials Science, Moscow State University, 119992, Moscow, Russia, State Scientific Center Karpov Institute of Physical Chemistry, 103063, Moscow, Russia, EMAT, University of Antwerp (RUCA), Groenenborgerlaan 171, B-2020, Antwerp, Belgium, and Institute of Solid State Chemistry, Pervomayskaia 91, Yekaterinburg 620219, Russia

Received February 26, 2003. Revised Manuscript Received May 13, 2003

Structural, chemical, and physical properties of whitlockite-type $Ca_9Bi(VO_4)_7$ were studied by X-ray powder diffraction (XRD), electron diffraction (ED), second-harmonic generation (SHG), thermogravimetry, differential scanning calorimetry, dielectric, and electrical-conductivity measurements. A new phase-transition of the ferroelectric type was found in $Ca_9Bi(VO_4)_7$ with a transition temperature, T_c, of 1053 ± 3 K. The polar phase, β-$Ca_9Bi(VO_4)_7$, is stable below T_c down to at least 160 K. The centrosymmetric β'-phase is stable above T_c up to 1273 ± 5 K. Above 1273 K, it decomposes to give $BiVO_4$ and whitlockite-type solid solutions of $Ca_{9+1.5x}Bi_{1-x}(VO_4)_7$. The $\beta \leftrightarrow \beta'$ phase transition is reversible and of second order. Electrical conductivity of β'-$Ca_9Bi(VO_4)_7$ is rather high ($\sigma = 0.6 \times 10^{-3}$ S/cm at 1200 K) and obeys the Arrhenius law with an activation energy of 1.0 eV. Structure parameters of $Ca_9Bi(VO_4)_7$ are refined by the Rietveld method from XRD data measured at room temperature (space group $R3c$; $Z = 6$; $a = 10.8992(1)$ Å, $c = 38.1192(4)$ Å, and $V = 3921.6(1)$ Å^3; $R_{wp} = 3.06\%$ and $R_p = 2.36\%$). Bi^{3+} ions together with Ca^{2+} ions are statistically distributed among the M1, M2, M3, and M5 sites. $Ca_9Bi(VO_4)_7$ has a SHG efficiency of about 140 times that of quartz. Through the powder SHG measurements, we estimated the nonlinear optical susceptibility, $\langle d \rangle$, at about 6.1−7.2 pm/V. This value for $Ca_9Bi(VO_4)_7$ is comparable with that for known nonlinear optical materials such as $LiNbO_3$ and $LiTaO_3$.

Introduction

Materials with an enhanced nonlinear optical (NLO) response, in particular second-harmonic-generating (SHG) materials, continue to attract much attention because of their great importance for optoelectronics. Objects of special interest are materials that combine NLO activity with ferroelectric or ionic-conductive properties, for example, compounds belonging to the $KTiOPO_4$ (KTP) family. New compounds with NLO activity have been recently explored among a group of the whitlockite-type[1] vanadates and phosphates, $Ca_9R(EO_4)_7$ (R = Al, Sc, Cr, Fe, Ga, Y, In, La−Lu, and Bi; E = P and V).[2−5] $Ca_9Bi(VO_4)_7$ has demonstrated SHG efficiency conversion of Nd-laser radiation of about 3 times that of KH_2PO_4.[2] Large single crystals of $Ca_9Bi(VO_4)_7$ were obtained and detailed processes of their growth were described.[6,7] Apart from remarkable results on NLO activity of $Ca_9R(EO_4)_7$, there were experimental evidences for ferroelectricity and ionic (Ca^{2+} or H^+ ions) conductivity in many phosphates and vanadates with the whitlockite-type structure.[3−5,8−10]

At room temperature (RT), calcium vanadate $Ca_3(VO_4)_2$ (space group $R3c$, $Z = 21$)[11] can be found in one modification isotypic with β-$Ca_3(PO_4)_2$.[12] In $Ca_3(VO_4)_2$[11]

* Corresponding author. Tel: 7-095-939-21-38. Fax: 7-095-939-21-58. E-mail: lazoryak@tech.chem.msu.ru.
† Department of Chemistry, Moscow State University.
‡ Karpov Institute of Physical Chemistry.
§ Department of Materials Science, Moscow State University.
|| EMAT, University of Antwerp.
⊥ Institute of Solid State Chemistry.
Present address: Laboratory of Solid State Chemistry, Institute for Chemical Research, Kyoto University, Gokasho, Uji, Kyoto, 611-0011, Japan.

(1) Calvo, C.; Gopal, R. *Am. Mineral.* **1975**, *60*, 120.
(2) Sleight, A. W.; Huang, J. U.S. Patent 5,202,891, 1993.
(3) Lazoryak, B. I.; Belik, A. A.; Stefanovich, S. Yu.; Morozov, V. A.; Malakho, A. P.; Baryshnikova, O. V.; Leonidov, I. A.; Leonidova, O. N. *Dokl. Acad. Nauk* **2002**, *384*, 780. (Engl. Transl. *Dokl. Phys. Chem.* **2002**, *384*, 144).
(4) Morozov, V. A.; Belik, A. A.; Stefanovich, S. Yu.; Grebenev, V. V.; Lebedev, O. I.; Van Tendeloo, G.; Lazoryak, B. I. *J. Solid State Chem.* **2002**, *165*, 278.
(5) Lazoryak, B. I.; Morozov, V. A.; Belik, A. A.; Stefanovich, S. Yu.; Grebenev, V. V.; Leonidov, I. A.; Mitberg, E. B.; Davydov, S. A.; Lebedev, O. I.; Van Tendeloo, G. *Solid State Sci.* In press.
(6) Kim, H. K.; Kim, M. S.; Park, S. M.; Sleight, A. W. *J. Cryst. Growth* **2000**, *219*, 61.
(7) Kim, M. S.; Park, S. M.; Kim, H. K. *J. Ind. Eng. Chem.* **2000**, *6*, 144.
(8) Lazoryak, B. I.; Belik, A. A.; Kotov, R. N.; Leonidov, I. A.; Mitberg, E. B.; Karelina, V. V.; Kellerman, D. G.; Stefanovich, S. Yu.; Avetisov, A. K. *Chem. Mater.* **2003**, 15, 625.
(9) Leonidov, I. A.; Leonidova, O. N.; Surat, L. L.; Kristallov, L. V.; Perelyaeva, L. A.; Samigullina, R. F. *Russ. J. Inorg. Chem.* **2001**, *46*, 268.
(10) Leonidov, I. A.; Belik, A. A.; Leonidova, O. N.; Lazoryak, B. I. *Russ. J. Inorg. Chem.* **2002**, *47*, 357.
(11) Gopal, R.; Calvo, C. *Z. Kristallogr.* **1973**, *37*, 67.

10.1021/cm031043s CCC: $25.00
Published on Web 06/28/2003

and β-$Ca_3(PO_4)_2$,[12] Ca^{2+} ions occupy five independent sites: M1−M5. The M1−M3 (18*b*) and M5 (6*a*) sites are fully occupied while the M4 site (6*a*) is half-occupied. There is one vacant site, M6 (6*a*), in the structure.

We have studied the crystal structures of $Ca_9R(VO_4)_7$ (R = Y and La−Lu)[13−16] at RT and found them to be isotypic with $Ca_3(VO_4)_2$,[11] β-$Ca_3(PO_4)_2$,[12] and mineral whitlockite, $Ca_{18.19}Mg_{1.17}Fe_{0.83}H_{1.62}(PO_4)_{14}$.[1] In $Ca_9R(VO_4)_7$, specific distribution of rare-earth metals among the crystallographic sites M1−M5 of the $Ca_3(VO_4)_2$ structure was found.[13−16] Two groups of rare-earth metals have been selected[16] depending on this distribution. The first group includes rare-earth metals from La^{3+} to Eu^{3+}, and the second group includes rare-earth metals from Gd^{3+} to Lu^{3+} and Y^{3+}. In the first group, La^{3+}−Eu^{3+} ions are distributed among the M1, M2, and M3 sites together with the Ca^{2+} ions. In the second group, Gd^{3+}−Lu^{3+} and Y^{3+} ions are located at the M1, M2, and M5 sites together with the Ca^{2+} ions. The site occupancies by rare-earth metals change monotonically with decreasing radii from La^{3+} to Lu^{3+}.

Evans et al.[17] have studied the crystal structure of $Ca_9Bi(VO_4)_7$ at 120 K (space group *R*3, *Z* = 6). Bi^{3+} ions (together with Ca^{2+} ions) were found to be statistically distributed among the M1, M2, M3, and M5 sites of the $Ca_3(VO_4)_2$ structure.[11] Moreover, the M3 site in $Ca_9Bi(VO_4)_7$ appeared to be statistically splitted into two different sites. The M4 site is vacant in all the compounds of the sort.[13−17]

Also, the structure of $Ca_{1.29}Bi_{0.14}VO_4$ ($Ca_{9.03}Bi_{0.98}(VO_4)_7$) was solved using single-crystal data (measured at RT) in another space group, namely *R*3*c*.[18] According to this work, Bi^{3+} ions (together with Ca^{2+} ions) were statistically distributed among the M1, M2, and M3 sites though the quantities of Ca^{2+} and Bi^3 in the positions were not examined. In addition, the compositions deduced from the refinement deviated strongly from that of $Ca_9Bi(VO_4)_7$. The latter is related to the high temperatures at which the single crystals of $Ca_{1.29}Bi_{0.14}VO_4$ were obtained. However, it is known that $Ca_9Bi(VO_4)_7$ decomposes above 1273 K.[6,19] Some other whitlockite-like compounds are also unstable at high temperatures, e.g., $Ca_9La(PO_4)_7$ decomposes to $Ca_{9+1.5x}La_{1-x}(PO_4)_7$ and $Ca_3La(PO_4)_3$ above 1723 K.[20] Therefore, reliable information about the structure of $Ca_9Bi(VO_4)_7$ can be obtained only by using the samples prepared at relatively low temperature.

Nonreconstructive phase transitions have been found above RT in $Ca_3(VO_4)_2$.[21,22] Single-crystal investigations of the dielectric properties showed that the transition at T_c = 1383 K is of ferroelectric nature.[21] The phase transitions in $Ca_3(VO_4)_2$ were also studied by high-temperature Raman spectroscopy.[22] A symmetry change ($R3c \leftrightarrow R\bar{3}m$) was assumed at 1383 K. In the temperature range from 500 to 800 K, an order−disorder phase transition was suggested for $Ca_3(VO_4)_2$.[22] Recently we have found ferroelectric phase transitions in other whitlockite-type compounds: $Ca_9R(PO_4)_7$ (R = In[4] and Fe[5]), $Ca_{1.5}Sr_{1.5}(VO_4)_2$,[2323] and $Ca_{3-x}Nd_{2x/3}(VO_4)_2$ ($0 \le x \le 3/7$).[9,10] In solid solutions of $Ca_{3-x}Nd_{2x/3}(VO_4)_2$,[9,10] Ca^{2+}-ion conductivity decreases with increasing Nd^{3+} content. The phase transition temperature (1383 K for $Ca_3(VO_4)_2$ and 1198 K for $Ca_9Nd(VO_4)_7$) also decreases with increasing Nd^{3+} content in the solid solutions. $Ca_3(VO_4)_2$ has a rather high Ca^{2+}-ion conductivity of 6×10^{-3} S/cm at 1200 K.

In this paper, we studied for the first time a similar phase transition in $Ca_9Bi(VO_4)_7$ (CBVO). We examined in detail the properties of CBVO in the vicinity of the phase transition and discussed some structure−property relationships. We also refined the structure parameters of CBVO (prepared at 1173 K) from X-ray powder diffraction (XRD) data measured at RT.

Experimental Section

Synthesis. CBVO was prepared by the conventional ceramic technique from a stoichiometric mixture of $Ca_3(VO_4)_2$ and $BiVO_4$ in an alumina crucible in air at 1173 K for 50 h with several intermediate grindings.[24] The resultant product was monophasic (JCPDS PDF 46-404) as XRD data showed. $Ca_3(VO_4)_2$ and $BiVO_4$ were synthesized at 1200 K for 50 h from stoichiometric mixtures of $CaCO_3$ with V_2O_5 and Bi_2O_3 with V_2O_5, respectively. Their XRD patterns were identical to those for $Ca_3(VO_4)_2$ (JCPDS PDF 46-756) and $BiVO_4$ (JCPDS PDF 14-688).

Electron Diffraction. Electron diffraction (ED) was performed on powdered samples deposited on holey carbon grids. ED patterns were obtained in the temperature range 100−297 K in a Philips CM20 electron microscope equipped with a double-tilt cooling holder. The ED patterns along different zones were obtained by the standard technique. Energy dispersion X-ray (EDX) spectra were registered using a LINK-2000 microscope attachment.

XRD and Structure Refinement. XRD data were collected at RT with a Siemens D500 Bragg−Brentano-type powder diffractometer supplied with an incident-beam quartz monochromator for filtering Cu $K\alpha_1$ radiation and a Braun position-sensitive detector. The diffractometer worked at 30 kV and 30 mA. Table 1 summarizes the conditions of data collection.

XRD data for CBVO were analyzed by the Rietveld method with Rietan-2000.[25] Coefficients for analytical approximation to atomic scattering factors for Ca, Bi, V, and O were taken from International Tables, Vol. C.[26] The split pseudo-Voigt function of Toraya[27] was fit to each reflection profile, and an 11th-order Legendre polynomial was fit to the background. Partial profile relaxation[25] was applied to the first four reflections, 012, 104, 006, and 110, to improve fits of these reflections in the last stage of the refinement. No preferred orientation was observed on the XRD patterns of CBVO.

(12) Dickens, B.; Schroeder, L. W.; Brown, W. E. *J. Solid State Chem*. **1974**, *10*, 232.
(13) Belik, A. A.; Morozov, V. A.; Khasanov, S. S.; Lazoryak, B. I. *Crystallogr. Rep.* **1997**, *42*, 751.
(14) Belik, A. A.; Morozov, V. A.; Kotov, R. N.; Khasanov, S. S.; Lazoryak, B. I. *Crystallogr. Rep.* **2000**, *45*, 389.
(15) Belik, A. A.; Morozov, V. A.; Grechkin, S. V.; Khasanov, S. S.; Lazoryak, B. I. *Crystallogr. Rep.* **2000**, *45*, 728.
(16) Belik, A. A.; Grechkin, S. V.; Dmitrienko, L. O.; Morozov, V. A.; Khasanov, S. S.; Lazoryak, B. I. *Crystallogr. Rep.* **2000**, *45*, 896.
(17) Evans, J. S. O.; Huang, J.; Sleight, A. W. *J. Solid State Chem*. **2001**, *157*, 255.
(18) Kim, M. S.; Lah, M. S.; Kim, H. K. *Bull. Korean Chem. Soc.* **2002**, *23*, 98.
(19) Kim, M. S.; Park, S. M.; Kim, H. K. *J. Korean Chem. Soc.* **1999**, *43*, 547.
(20) Jungowska, W. *Solid State Sci.* **2002**, *4*, 229.
(21) Glass, A. M.; Abrahams, S. C.; Ballman, A. A.; Loiacono, G. *Ferroelectrics* **1978**, *17*, 579.
(22) Grzechnik, A. *Chem. Mater*. **1998**, *10*, 1034.
(23) Belik, A. A.; Stefanovich, S. Yu.; Lazoryak, B. I. *Mater. Res. Bull.* **2001**, *36*, 1873.
(24) Lazoryak, B. I.; Dmitrienko, L. O.; Grechkin, S. V. *Russ. J. Inorg. Chem*. **1990**, *35*, 617.
(25) Izumi, F.; Ikeda,T. *Mater. Sci. Forum* **2000**, *321−324*, 198.
(26) Maslen, E. M.; Fox, A. G.; O'Keefe, M. A. *International Tables for Crystallography*; Kluwer: Dordrecht, The Netherlands, 1999; Vol. C, pp 572−574.
(27) Toraya, H. *J. Appl. Crystallogr*. **1990**, *23*, 485.

Table 1. Important Refined Parameters and Counting Conditions for $Ca_9Bi(VO_4)_7$

space group	*R*3*c* (No. 161)
Z	6
2θ range (deg)	9−140
step width (deg)	0.02
I_{max} (counts)	37473
lattice parameters	
a (Å)	10.8992(1)
c (Å)	38.1192(4)
V (Å^3)	3921.6(1)
No. of Bragg reflections	1634
variables	
structure/lattice	68/2
reliable factors	
R_{wp}; R_p	3.06%; 2.36%
R_I; R_F	2.52%; 1.8%
S	1.23

Isotropic atomic displacement parameters, *B*, with the isotropic Debye−Waller factor formulated as $\exp(-B\sin^2\theta/\lambda^2)$ were assigned to all the sites.

Physical and Chemical Properties. The temperature dependence of SHG responses for the powder samples of CBVO (main grain size of about 5 μm) was measured in reflection mode with a Q-switch pulsed YAG:Nd laser with a wavelength, λ_ω, of 1064 nm. An α-SiO_2 powder kept at RT with 3−5 μm grain size served as a reference material. A detailed description of the equipment and the methodology used has been published elsewhere.[28]

Thermogravimetric (TG) and differential-scanning-calorimetric (DSC) measurements were performed in the temperature range of 293−1473 K using a Netzsch STA 409 thermoanalyzer with kaolin as a reference sample and a heating rate of 10 K/min.

Ceramic samples of CBVO were used for dielectric and electrical-conductivity investigations. Disklike pellets (0.5−1.5 mm long and 5−6 mm diam) were prepared by pressing and sintering at 1273 K for 2 h. The densities of the ceramic samples rose to 90% of the theoretical density. A Pt paste was put on flat surfaces of the pellets and then they were heated to 923 K to produce metal electrodes. The dielectric constant (ϵ) and the loss tangent (tan δ) were measured with computer-controlled AC-bridges R5083 and E7-12 at electric-field frequencies between 10 kHz and 1 MHz and in a temperature range from 160 to 1200 K. For the impedance spectroscopy measurements in a frequency range of 1−10^7 Hz at 300−1300 K, we used a Solatron 1260 frequency response analyzer. DC-conductivities, σ, were obtained from the calculation of parameters of an equivalent electric circuit.

Results

Sample Composition. Quantitative EDX analysis performed inside the electron microscope shows that the Ca/Bi ratio remains practically constant across the sample and is equal to the theoretical value (Ca/Bi = 9). This result indicates a good composition uniformity of the obtained material.

Thermal Stability. Figure 1 shows part of the TG, DSC, and DDSC (derivative of DSC signal on time) curves for CBVO during heating. According to the TG data, the sample weight does not change from 300 to 1473 K. The DSC and DDSC data show that three temperature ranges can be distinguished for CBVO: (1) below 1273 ± 5 K, (2) between 1273 and 1433 K, and (3) above 1433 K.

When CBVO is quenched from 1273 K to RT, the XRD pattern contains only reflections of the whitlockite-type phase with a composition $Ca_9Bi(VO_4)_7$ (Figure 2). Annealing CBVO above 1273 K followed by quenching to RT leads to the appearance of $BiVO_4$ in addition to a whitlockite-type phase (Figure 2). Because no other phases are detected, the composition of the whitlockite-type phase can be presented as $Ca_{9+1.5x}Bi_{1-x}(VO_4)_7$. Solid solutions of $Ca_{9+1.5x}Bi_{1-x}(VO_4)_7$ are formed in a compositional range $0 \le x \le 0.98$.[19] The quantity of $BiVO_4$ increases with increasing the temperature of annealing. These facts point to a thermal stability of CBVO between 273 and 1273 K in air. According to the DSC and XRD data, CBVO decomposes to $BiVO_4$ and whitlockite-type solid solutions of $Ca_{9+1.5x}Bi_{1-x}(VO_4)_7$ above 1273 K. The exothermic effects on both DSC and DDSC curves indicate that the *subsolidus* temperature for a sample with nominal composition $Ca_9Bi(VO_4)_7$ is 1433 ± 5 K.

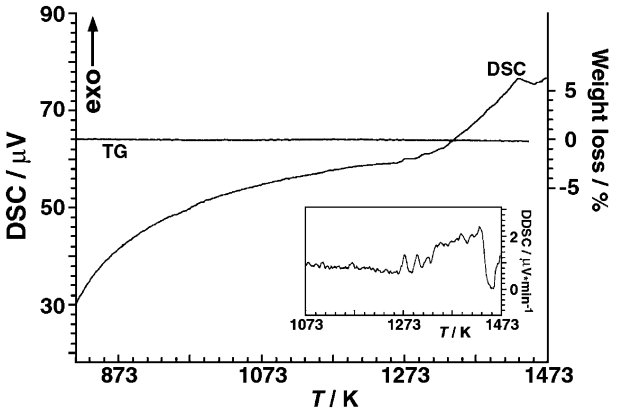

Figure 1. TG, DSC, and DDSC (inset) curves for $Ca_9Bi(VO_4)_7$.

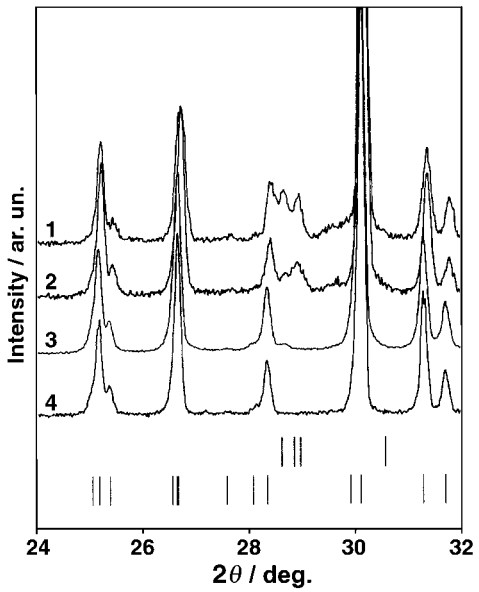

Figure 2. XRD patterns in a 2θ range of 24−32° for different samples of $Ca_9Bi(VO_4)_7$ quenched to room temperature from (1) 1553 K, (2) 1473 K, (3) 1373 K, and (4) 1273 K. Bragg reflections for $BiVO_4$ (ICDD, PDF 14-688; upper) and $Ca_9Bi(VO_4)_7$ (ICDD, PDF 46-404; lower) are indicated by tick marks.

Electron Diffraction. The [0001]*, [10$\bar{1}$0]*, and [11$\bar{2}$0]* ED patterns at RT for CBVO are shown in Figure 3. The spots on the ED patterns could be indexed in a trigonal system with lattice parameters determined by XRD (JCPDS PDF 46-404). The [11$\bar{2}$0]* diffraction

(28) Stefanovich, S. Yu. *Lasers and Electrooptics (CLEO−Europe 94)*; Elsevier: Amsterdam, The Netherlands, 1994; p 249.

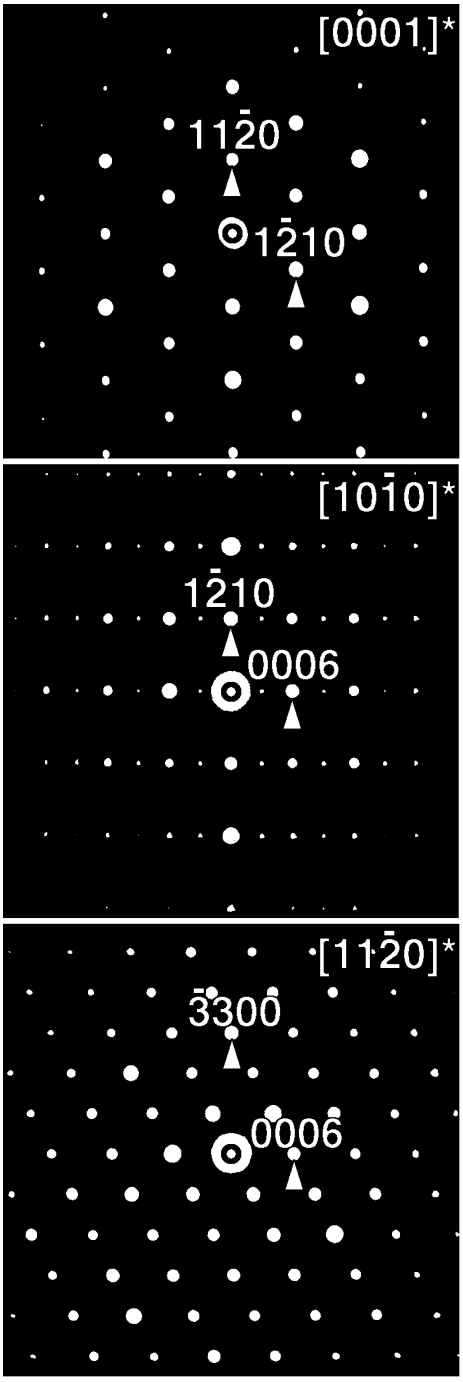

Figure 3. Electron diffraction patterns along the [0001], [10$\bar{1}$0], and [11$\bar{2}$0] zone axes for $Ca_9Bi(VO_4)_7$ at room temperature.

pattern exhibits a rhombohedral shift of the spot rows along $\boldsymbol{c}^*$ by $h\ c^*/3$. Reflection conditions derived were $-h + k + l = 3n$ for $hkil$, $h + l = 3n$ and $l = 2n$ for $h\bar{h}0l$, $l = 3n$ for $hh\overline{2h}l$, and $l = 6n$ for $000l$ (hexagonal axes, obverse setting) affording one noncentrosymmetric space group of $R3c$. The presence of spots with $l = 3n$ ($n = 2m + 1$) for $000l$ on the [10$\bar{1}$0]* diffraction pattern can be explained by the double diffraction. Indeed, intensities of these reflections are systematically lower than those with $l = 6n$, and on tilting the sample around the [$000l$] axis these reflections further weaken and vanish. In addition, reflections with $l = 3n$ ($n = 2m + 1$) for $000l$ were not observed on the [11$\bar{2}$0]* diffraction pattern.

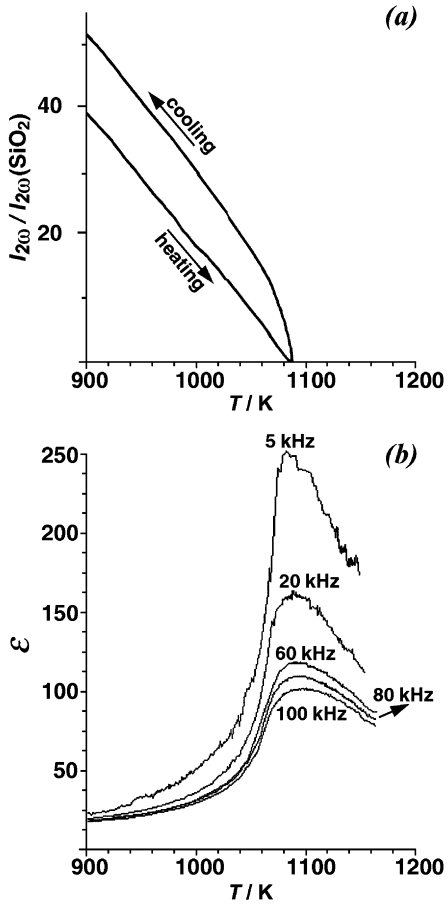

Figure 4. Temperature dependencies of the SHG signals (*a*) and the dielectric permittivity (ϵ) (*b*) at different electric-field frequencies for $Ca_9Bi(VO_4)_7$.

At 120 K, CBVO was reported to have the space group $R3$.[17] In our case, cooling the sample from 297 to 100 K did not change the ED patterns. The crystal symmetry of CBVO, therefore, does not change in the temperature range from 100 to 297 K.

Second-Harmonic Generation. Fragments of the temperature dependence of the SHG responses for CBVO are shown in Figure 4a. Full curves as well as the SHG signals at RT ($I_{2\omega} \sim 140$) were reported earlier.[3]

On heating, the SHG signals vanish above (1058 ± 3) K. The disappearance of the SHG signals indicates that above 1058 K the structure of CBVO possesses a center of symmetry. On cooling, the SHG signals reappear at the same temperature, indicating the existence of a completely reversible second-order polar-to-centrosymmetric phase transition with transition temperature $T_c = 1058 \pm 3$ K. More support for a second-order phase transition follows from the more gradual than steplike changes of the SHG signals when approaching T_c. A certain discrepancy between the SHG intensities on heating and cooling may be attributed to changes in the domain structure of the sample during thermal cycling.

Dielectric and Electrical-Conductivity Data. The temperature dependence of the dielectric permittivity for CVBO at different electric-field frequencies (Figure 4b) demonstrates maxima at the same temperature of 1053 ± 3 K. The characteristic shapes of the maxima and the independence of the temperature of the ϵ

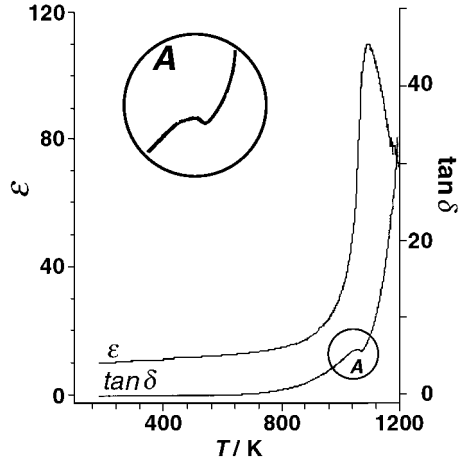

Figure 5. Temperature dependencies of the dielectric permittivity (ϵ) and loss tangent (tanδ) for $Ca_9Bi(VO_4)_7$ in the temperature range from 160 to 1200 K at 60 kHz. Inset *A* shows a maximum on the tanδ versus *T* curve.

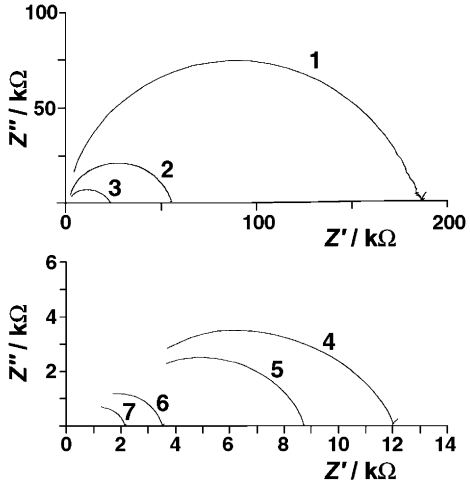

Figure 6. Complex impedance diagrams for $Ca_9Bi(VO_4)_7$ at (1) 973 K, (2) 1020 K, (3) 1060 K, (4) 1083 K, (5) 1112 K, (6) 1170 K, and (7) 1209 K.

maximum, $T(\epsilon_{max})$, of the electric-field frequencies have allowed us to classify the phase transformation as a ferroelectric phase transition.

The broadened maximum below T_c on the tanδ versus *T* curve (Figure 5) may be attributed to an increased mobility of the polar domains in the vicinity of ferroelectric Curie temperature. This explanation is also in accordance with the above-mentioned influence of the domain structure on the SHG signals. Apart from the ferroelectric-type peaks at T_c on the ϵ versus *T* curves, and the maximum below T_c on the tanδ versus *T* curve, no other dielectric anomalies have been registered in the temperature range of 160−1200 K (Figure 5); i.e., no additional phase transitions were observed in CBVO in the temperature range between 160 and 1200 K. Moreover, the ϵ value near T_c strongly depends on the electric-field frequency. An increase of the electric-field frequency leads to a decrease of the ϵ value and washing out its maximum near T_c (Figure 4). This type of behavior is typical for ferroelectrics with an increased ionic conductivity.

Figure 6 shows the complex electrical impedance diagrams for CBVO at different temperatures. The impedance diagram consists of one deformed semicircle

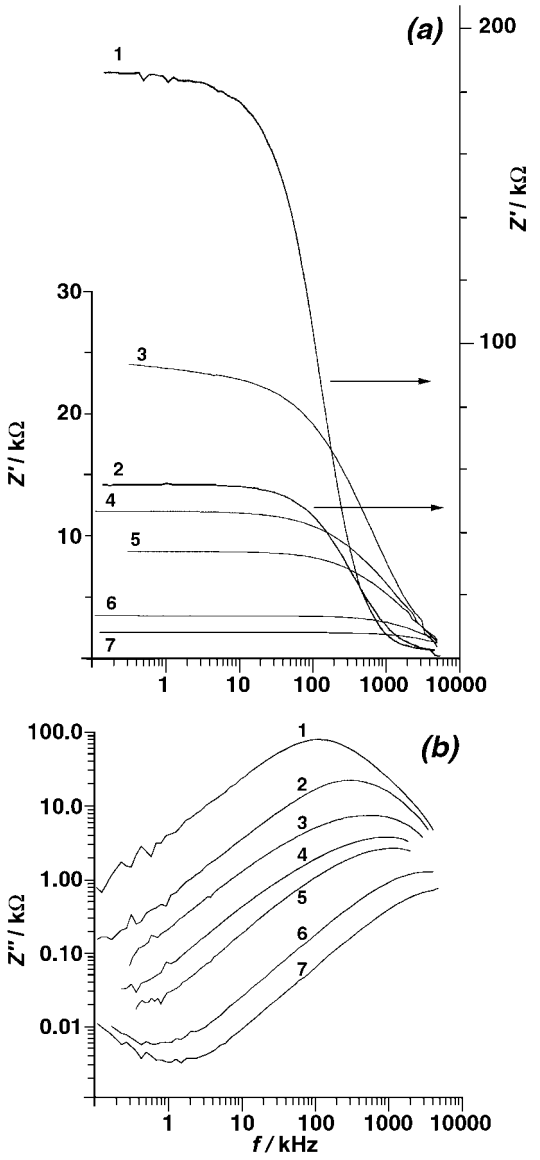

Figure 7. Frequency dependence of the (*a*) real and (*b*) imaginary parts of the complex impedance of $Ca_9Bi(VO_4)_7$ at (1) 973 K, (2) 1020 K, (3) 1060 K, (4) 1083 K, (5) 1112 K, (6) 1170 K, and (7) 1209 K.

often observed in polycrystalline solid-state electrolytes. The frequency dependence of the real (Z') and imaginary (Z'') part of the complex impedance is shown in Figure 7. The Z' and Z'' parts depend on the electric-field frequency ($f = \omega/2\pi$) and in a first approximation are described by the formula

$$Z' = R/[1 + (\omega CR)^2] \text{ and } Z'' = \omega CR^2/[1 + (\omega CR)^2]$$

where *R* is the sample resistance on direct current and *C* is the sample capacity. The value of Z'' for the low-frequency region (when $(\omega CR)^2 < 1$ and $Z' = R$) increases with increasing frequency, whereas at high frequencies ($(\omega CR)^2 > 1$), Z' sharply decreases and Z'' decreases according to $\sim 1/f$. The increased values of Z'' at high temperatures and low frequencies are due to the contribution of the electrode impedance.

Because only one deformed semicircle was observed on the complex impedance (Figure 6), the equivalent electric circuit related to the sample was presented by parallel circuits (R_bC_b), where R_b ($\sigma = 1/R_b$) and C_b are

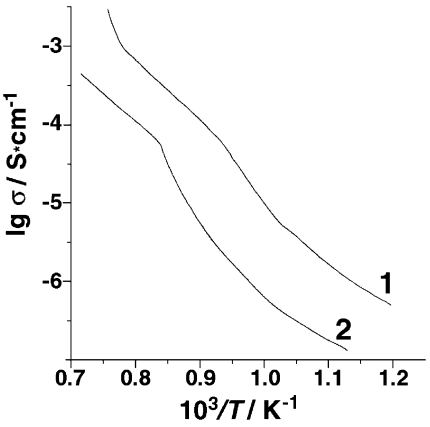

Figure 8. Plots of lgσ versus $10^3/T$ in (1) $Ca_9Bi(VO_4)_7$ and (2) $Ca_9Nd(VO_4)_7$. Unit of σ: S cm^{-1}.

resistance and capacitance of the grains. Thus, only volumetric resistance and capacitance of polycrystalline grains define impedance of the sample in the frequency range of $1-5 \times 10^3$ kHz. The absence of a noticeable influence of the resistance of grain boundaries on ionic conductivity is proved by the following data. During the $\beta \rightarrow \beta'$ phase transition the ionic conductivity in CBVO is noticeably changeable, while the grain boundaries in β- and β'- phases are almost the same. These results indicate that an input of the resistance of grain boundaries into conductivity is very insignificant.

The lgσ versus T^{-1} curves (lgσ = log σ) for CBVO and $Ca_9Nd(VO_4)_7$[9,10] are shown in Figure 8. The ferroelectric phase transition in CBVO is accompanied by a change of the curve slope, i.e., the temperature range where the curve slope changes (1055−1063 K) coincides with T_c. In the heating−cooling cycle, this change in the lgσ versus T^{-1} curve occurs without any hysteresis.

Above T_c, the electrical conductivity in CBVO obeys the Arrhenius law with an activation energy (≈1.0 eV) very close to that of the Ca^{2+}-ion conductor, $Ca_9Nd(VO_4)_7$ (Figure 8).[9,10] In CBVO at 1200 K, the electrical conductivity is about 8 times larger than that in $Ca_9Nd(VO_4)_7$. In addition, the electrical conductivity in CBVO starts to increase notably above 1300 K in contrast to that of $Ca_9Nd(VO_4)_7$. Apparently, this increase in conductivity is caused by the decomposition of CBVO above 1273 K.

Crystal Structure of CBVO at 293 K. As the initial fractional coordinates in the Rietveld analysis of CBVO, we used those of $Ca_9Nd(VO_4)_7$ (space group $R3c$, No. 161).[15] Preliminary refinements have shown that Bi^{3+} ions together with Ca^{2+} ions occupy the M1−M3 and M5 sites of the structure. Indeed, the following occupancies, g, were obtained in the assumption that these sites are occupied only by Ca^{2+} ions: g(Ca) = 1.237(6) with B = 0.63(7) Å^2 for M1, g(Ca) = 1.359(8) with B = 0.57(7) Å^2 for M2, g(Ca) = 1.489(8) with B = 2.65(7) Å^2 for M3, and g(Ca) = 1.125(11) with B = 0.86(11) Å^2 for M5. The refinement of the g value for the M4 site when Ca^{2+} ions are located in this site gives g(Ca) = 0.020(9) with fixed B = 2.0 Å^2. In the next stage of the structure refinement, the distribution of the Bi^{3+} ions among the M1−M3 and M5 sites is refined with the assumption that these sites are fully occupied, that is, g(Ca) + g(Bi) = 1 for the M1−M3 and M5 sites. The M4 site is supposed to be vacant. The composition obtained in this model is very close to the stoichiometric one (the total number of Bi^{3+} ions is 6.12 per unit cell). But the B parameter for the M3 site is enlarged, B(M3) = 3.18(8) Å^2, in comparison with those of other sites: B(M1) = 0.88(7) Å^2, B(M2) = 0.96(7) Å^2, and B(M5) = 0.95(12) Å^2. The occupancies of the M3 site in this case are g(Ca) = 0.851(3) and g(Bi) = 0.149. In analogy with results obtained by Evans et al. for CBVO,[17] we assumed that cations at the M3 site are disordered between two close positions, M31 and M32. The refinement of the distribution of the virtual atom, VA = $0.851Ca^{2+}$ + $0.149Bi^{3+}$, between the M31 and M32 sites gives g(VA) = 0.495(3) for M31 and g(VA) = 0.505 for M32 with common B = 1.65(8) Å^2. Thus, the M31 and M32 sites have almost the same occupancy. The model into which the M31 and M32 sites are introduced yields more reasonable B parameters for M31 and M32 and lower R factors.

At a last stage of the structure refinement, the following linear constraints are imposed on the oc-

Table 2. Fractional Coordinates and Isotropic Atomic Displacement Parameters for $Ca_9Bi(VO_4)_7$

atom[a]	x	y	z	B (Å^2)
M1	0.7248(3)	0.8596(3)	0.4307(2)	0.94(7)
M2	0.6163(2)	0.8240(3)	0.2350(2)	0.99(7)
M31	0.1314(7)	0.2582(6)	0.3182(2)	1.66(12)
M32	0.1245(7)	0.2801(6)	0.3269(2)	= B(M31)
M5	0	0	0	1.11(12)
V1	0	0	0.2672(2)	1.18(10)
V2	0.6836(2)	0.8574(3)	0.1340(2)	0.46(7)
V3	0.6519(3)	0.8470(4)	0.0322(2)	0.90(8)
O1	0	0	0.3124(5)	3.0(4)
O2	0.0119(10)	0.8522(8)	0.2569(3)	0.3(2)
O3	0.7139(12)	0.9069(12)	0.1762(4)	2.7(3)
O4	0.7676(12)	0.7648(12)	0.1217(3)	1.4(3)
O5	0.7273(12)	0.0189(11)	0.1121(3)	0.6(2)
O6	0.5042(9)	0.7497(14)	0.1235(3)	1.2(2)
O7	0.5953(12)	0.9545(12)	0.0453(4)	1.2(3)
O8	0.5708(11)	0.6820(11)	0.0518(3)	0.7(2)
O9	0.8331(10)	0.9291(14)	0.0434(3)	1.0(2)
O10	0.6282(9)	0.8241(12)	0.9885(3)	1.4(2)

[a] g(Ca) = 0.93(2) and g(Bi) = 0.07(2) for the M1 site; g(Ca) = 0.89(2) and g(Bi) = 0.11(2) for the M2 site; g(Ca) = 0.43(2) and g(Bi) = 0.07(2) for the M31 and M32 sites; and g(Ca) = 0.96(2) and g(Bi) = 0.04(2) for the M5 site.

Table 3. Bond Lengths (Å) in $Ca_9Bi(VO_4)_7$

bond		bond	
M1−O2	2.487(9)	M31−M32	0.438(10)
−O4	3.071(12)	M31−O1	2.448(6)
−O5	2.574(12)	−O2	2.615(11)
−O6	2.438(14)	−O3	3.066(12)
−O6a	2.520(14)	−O4	2.339(13)
−O7	2.386(12)	−O5	2.337(12)
−O8	2.254(11)	−O7	2.641(13)
−O10	2.384(8)	−O8	2.934(11)
M2−O2	2.343(10)	−O10	2.522(13)
−O3	2.451(11)	−O10a	2.742(13)
−O4	2.345(10)	M32−O1	2.707(6)
−O5	2.282(11)	−O2	3.042(11)
−O7	2.862(11)	−O3	2.703(12)
−O8	2.862(11)	−O4	2.495(13)
−O9	2.485(15)	−O5	2.378(12)
−O9a	2.550(14)	−O7	2.451(13)
M5−O6 (×3)	2.305(11)	−O8	2.586(13)
−O9 (×3)	2.288(12)	−O10	2.669(13)
V1−O1	1.720(17)	−O10a	2.785(13)
−O2 (×3)	1.725(8)	V3−O7	1.651(11)
V2−O3	1.675(12)	−O8	1.728(11)
−O4	1.732(10)	−O9	1.765(9)
−O5	1.785(10)	−O10	1.686(10)
−O6	1.752(9)		

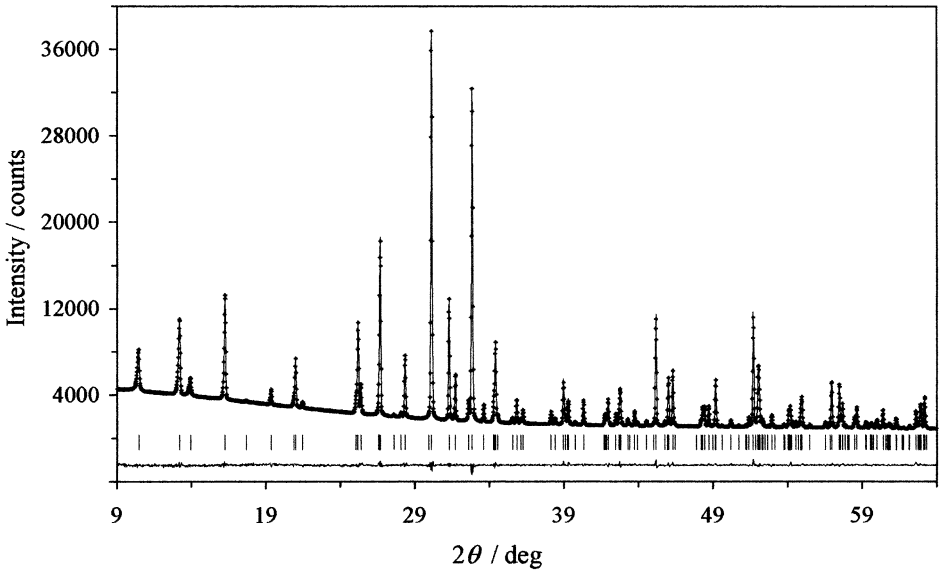

Figure 9. Portion of observed (crosses), calculated (solid line), and difference XRD patterns in a 2θ range of 9−64° for β-$Ca_9Bi(VO_4)_7$. Tick marks denote the peak positions of possible Bragg reflections.

cupancies: (1) $g(Ca) + g(Bi) = 1$ for the M1, M2, and M5 sites, (2) the M4 site is vacant, (3) the overall occupancies of the M31 and M32 sites are equal to each other, and (4) $g(Ca) + g(Bi) = 0.5$ for the M31 and M32 sites. The Rietveld refinement with these constraints gives 5.98 Bi^{3+} ions per unit cell. The distribution of Bi^{3+} ions found in this work from XRD data is close to that obtained from single-crystal data.[17] Table 1 lists the experimental/refinement conditions, final *R* factors, and structural data. Final fractional coordinates and *B* parameters are given in Table 2, and metal−oxygen bond lengths are given in Table 3. Figure 9 displays the observed, calculated, and difference XRD patterns for CBVO.

Discussion

A high-temperature phase transition of the ferroelectric type at $T_c = 1053 \pm 3$ K was found in CBVO using the SHG, dielectric, and electrical conductivity measurements. The polar phase, β-CBVO, is stable below T_c to at least 160 K, whereas the centrosymmetric high-temperature phase, β'-CBVO, is stable above T_c up to 1273 ± 5 K. β'-CBVO could not be obtained by quenching from high temperatures to RT. These new data substantially enrich the picture of electric phenomena in whitlockite-type phosphates and vanadates, which has been described in our previous works.[3−5,9,10,23,29]

Particularly, we found that all compounds $Ca_9R(VO_4)_7$ (R = Y, La−Lu, and Bi) exhibit a ferroelectric to ionic-conductor phase transition[3] similar to that found earlier for members of the KTP structural family.[30] However, structural changes at the $\beta \rightarrow \beta'$ phase transition in all whitlockite-type vanadates are quite different from the KTP-type structure and assumed to be similar with the $\beta \rightarrow \beta'$ phase transition observed in $Ca_9R(PO_4)_7$ (R = In[4] and Fe[5]).

The distinctive feature of the $\beta \rightarrow \beta'$ phase transition is the reorientation of half of the V_1O_4 tetrahedra.[3] Such structural mechanism can be directly correlated with the ferroelectric anomaly of the permittivity at T_c, but cannot explain either the high NLO in CBVO below T_c or ionic conductivity at higher temperature.

The $\beta \leftrightarrow \beta'$ phase transition in $Ca_3(VO_4)_2$ is accompanied by a 3−4 times increase of the ionic conductivity.[10] Figure 8 shows a similar increase of σ at T_c in $Ca_9Nd(VO_4)_7$ and CBVO. In the latter two compounds, the ionic conductivity over the temperatures of their phase transitions become almost twenty times higher, though absolute values of the conductivity are significantly lower in comparison with $Ca_3(VO_4)_2$. In CBVO with its lowest T_c, the conductivity exceeds (ca. 8 times) corresponding values for $Ca_9Nd(VO_4)_7$.

The ionic conductivity in CBVO can be explained by the structural data and the comparison of CBVO characteristics with similar data for $Ca_3(VO_4)_2$ and $Ca_{3-x}Nd_{2x/3}(VO_4)_2$.[10] These phases differ only by the occupation of the M4 site. The M4 site of the whitlockite-type structure is vacant in CBVO while it is partially occupied in $Ca_3(VO_4)_2$ (half-occupation) and solid solutions of $Ca_{3-x}Nd_{2x/3}(VO_4)_2$. It has also been demonstrated that the Ca^{2+} ion migration in the whitlockite-type structure of $Ca_3(VO_4)_2$ and solid solutions of $Ca_{3-x}Nd_{2x/3}(VO_4)_2$ is notably influenced by the cation distribution over the structural positions.[10]

In the whitlockite-type structure, calcium cations primarily migrate by two paths: (I) $(-M4-M2-M4'-)_\infty$ and (II) $(-M3-M4-M3'-M6-M3''-)_\infty$.[10] In $Ca_9Nd(VO_4)_7$ and CBVO in contrast to $Ca_3(VO_4)_2$, some Ca^{2+} cations in the M2 and M3 sites are replaced by Bi^{3+} or Nd^{3+}. Therefore, the M2 and M3 sites occupied by Bi^{3+} or Nd^{3+} cations are blocked for the migration of Ca^{2+} cations. Such blockage of part of the M2 and M3 sites leads to a decrease of the ionic conductivity in $Ca_9R(VO_4)_7$ (R = Bi and Nd) in comparison with that of $Ca_3(VO_4)_2$.[10] A decrease of the occupation degree of the M2 and M3 sites by R^{3+} cations from 0.2 (for Nd^{3+})[9] to ~0.14 (for Bi^{3+}) leads to an increase of the conductivity. The

(29) Leonidov, I. A.; Khodos, M. Ya.; Fotiev, A. A.; Zhukovskaya, A. S. *Inorg. Mater.* **1988**, *24*, 347. (Engl. Transl. **1988**, *24*, 280).
(30) Stefanovich, S. Yu.; Mill, B. V.; Belokoneva, E. I. *Ferroelectrics* **1996**, *185*, 63.

distribution of Bi^{3+} cations in the CBVO structure differs by the partial occupation of the M5 site.

Apparently, the disordering of the M3 site in CBVO also increases the mobility of calcium cations in the structure. A noticeable increase of the conductivity at the phase transition temperature (T_c) for $Ca_9Nd(VO_4)_7$ and CBVO is connected with the transition from β- to β'-. The equivalence of the M1 and M2 sites in the β'-phase[4,5] leads to an increase of the number of accessible sites for Ca^{2+} transportation and a noticeable conductivity growth.

Optical second harmonic measurements made in the present work on powder samples of CBVO confirm a very strong SHG signal previously observed by Sleight et al.[2] for small crystals. A more comprehensive analysis of SHG activity of the material suggests evaluation of the second-order susceptibility tensor d. The tensor of the NLO susceptibility is a more fundamental characteristic of a NLO material than the intensity ($I_{2\omega}$) of the SHG signal. Estimation of the average value of the tensor ($\langle d \rangle$) is possible using the fact that in fine powders the so-called coherent length (l) is restricted by the grain dimension (ca. 5 μm in our case). The reference material α-SiO_2 has the same grain size. It allows us to omit l values from the relative calculations and to use a simple expression obtained earlier[28] for fine powders

$$\langle d \rangle / d_{11}(SiO_2) = Const(n + 1)^3/(n_{SiO2} + 1)^3 \sqrt{I_{2\omega}}$$

Here n stands for an average refraction index of the substance under investigation, and the geometric factor *Const* stands for unity, reflecting directional averaging of the crystallite orientations. The $\langle d \rangle$ value for CBVO can be estimated using $n_{SiO2} = 1.54$ and $d_{11}(SiO_2) = 0.364$ pm/V. $I_{2\omega}$ is the measured SHG intensity with respect to α-SiO_2. Taking into account that $I_{2\omega}$ for different CBVO powders ranges between 140 and 200 and $n = 1.85$ for CBVO crystals[7] and assuming *Const* $= 1$, we obtain $\langle d \rangle \approx 6.1-7.2$ pm/V for CBVO. Despite the roughness of the estimation, we can place CBVO on one level with such famous nonlinear optical materials as $LiNbO_3$ and $LiTaO_3$.

Acknowledgment. This work was supported by the Russian Foundation for Basic Research (Grant 03-03-32779). V.A.M. is grateful to DWTC (Belgium) for financial support. Part of this work is supported by IUP V-1. We thank Dr. S. S. Khasanov (Institute of Solid State Physics, Russia) for XRD measurements.

CM031043S